

The Case for a 700+ GeV WIMP: Cosmic Ray Spectra from ATIC and PAMELA

Ilias Cholis,¹ Gregory Dobler,² Douglas P. Finkbeiner,² Lisa Goodenough,¹ and Neal Weiner¹

¹*Center for Cosmology and Particle Physics,*

Department of Physics, New York University, New York, NY 10003

²*Harvard-Smithsonian Center for Astrophysics,*

60 Garden St., Cambridge, MA 02138

(Dated: March 8, 2019)

Abstract

Multiple lines of evidence indicate an anomalous injection of high-energy e^+e^- in the Galactic halo. The Advanced Thin Ionization Calorimeter (ATIC) has detected an excess bump in the electron cosmic ray spectrum from 300-800 GeV, falling back to the expected $E^{-3.2}$ power law at 1 TeV and above. The recent e^+ fraction spectrum from the Payload for Antimatter Matter Exploration and Light-nuclei Astrophysics (PAMELA), shows a sharp rise up to 80 GeV. Excess microwaves towards the Galactic center in the WMAP data are consistent with hard synchrotron radiation from a population of 10-100 GeV e^+e^- (the WMAP “haze”). We argue that dark matter annihilations can provide a consistent explanation of all of these data, focusing on dominantly leptonic modes, either directly or through a new light boson. Normalizing the signal to the highest energy evidence (ATIC), we find that similar cross sections provide good fits to PAMELA and the Haze, and that both the required cross section and annihilation modes are achievable in models with Sommerfeld-enhanced annihilation. These models naturally predict significant production of gamma rays in the Galactic center via a variety of mechanisms. Most notably, there is robust inverse-Compton scattered (ICS) gamma-ray signal arising from the energetic electrons and positrons, detectable at Fermi/GLAST energies, which should provide smoking gun evidence for this production.

I. INTRODUCTION

The search for astrophysical signatures of WIMP annihilation has blossomed in recent months, with tantalizing announcements of electron and positron cosmic-ray spectra by two projects. Unexpected features in such spectra are of great interest for particle physics, because of the possibility that WIMP annihilation products could be observed this way.

The first project, ATIC, has measured the spectrum of $e^+ + e^-$ (ATIC cannot distinguish e^+ from e^-) from 20 to 2000 GeV, finding a broad bump at 300 – 800 GeV [1]. ATIC discriminates protons from electrons by comparing the shapes of the hadronic vs. electromagnetic showers within its bismuth germanate (BGO) calorimeter. The electron energy is measured two ways: by the total amount of energy deposited in the calorimeter (usually about 85% of the incoming electron energy) and by the position of shower maximum. Both techniques give consistent results[55], finding about 210 events at 300 – 800 GeV, compared to the 140 expected. This result confirms similar excesses seen previously by ATIC [2] and PPB-BETS [3]. Though suggestive, this alone would not be taken as strong evidence for WIMP annihilation, because there are astrophysical ways to accelerate electrons (SN shocks, pulsars, etc.). Dark matter annihilation would produce equal numbers of e^+ and e^- , so it is crucial to determine what fraction of the ATIC excess is positrons.

The second project, PAMELA [4], *can* distinguish between e^+ and e^- and finds a sharp rise in the flux ratio $\phi(e^+)/(\phi(e^+) + \phi(e^-))$ above 10 GeV, continuing up to 80 GeV [5]. This confirms previous indications of an excess by HEAT [6] and AMS-01 [7], but at much higher confidence. Although lower energies ($\lesssim 10$ GeV) are significantly affected by solar modulation, these high energy particles are not. The ordinary secondary positron spectrum, originating from cosmic ray (CR) interactions with the interstellar gas, is softer than the primary electron spectrum, so the positron fraction was expected to drop with energy. The surprising upturn in positron fraction, therefore, is very strong evidence for a primary source of positrons. While astrophysical sources such as pulsars offer alternative explanations [8, 9, 10, 11, 12], the amplitude and spectral shape of the positrons compel us to consider dark matter as an explanation.

Before proceeding, it is instructive to make a simple empirical connection between PAMELA and ATIC/PPB-BETS. For a casual observer of the PAMELA data, it seems clear that for energies between 10 and 80 GeV, the rise is well described by a power law. If

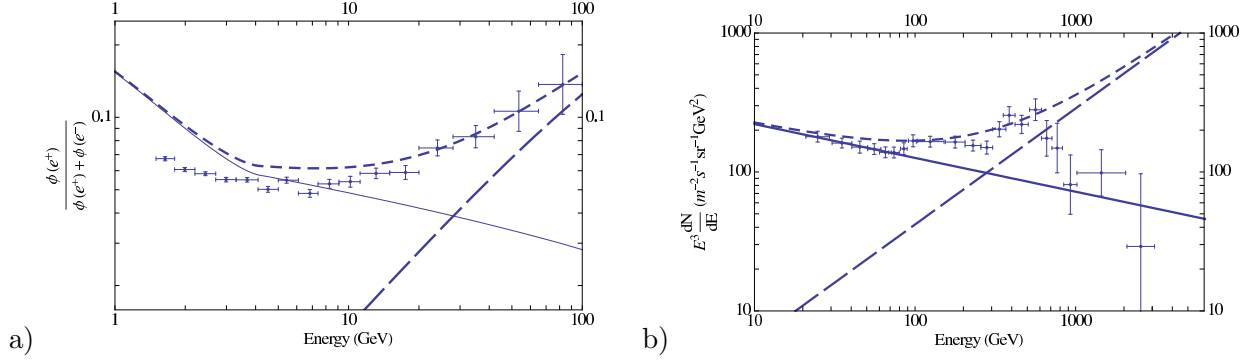


FIG. 1: (a) A new power-law component of e^+e^- fit to the PAMELA excess (*long-dashed*) with expected background e^+ model (*solid*) and total positron fraction (*short-dashed*). (b) Extrapolation of this new component to ATIC energies, assuming equal parts e^+ and e^- . For reference, the new component positrons are about 12% of the PAMELA fraction at 100 GeV, and therefore constitute about 1/4 of the ATIC flux $\phi(e^+) + \phi(e^-)$ at 100 GeV. The fact that the ATIC and PAMELA excesses are connected by such a generic argument suggests that a single mechanism, producing equal numbers of e^+ and e^- , explains both.

we assume that this new component provides equal numbers of electrons and positrons, it constitutes $\sim 25\%$ of the total electronic activity at 100 GeV (i.e. positrons are $\sim 12\%$ of the total). A natural exercise is to fit this rise, by assuming some new component of e^+e^- which scales as a power of energy. One can extrapolate this power law to higher energies and see where it makes an order unity contribution of electronic activity (i.e., where the positron fraction is $\gtrsim 30\%$). The extrapolation of PAMELA (Figure 1) naturally yields an excess in the range of ATIC and PPB-BETS similar to the one observed. While this argument is heuristic, it nonetheless makes a strong case that these signals arise from the same source, rather than *two* new independent sources of high energy e^+e^- coincidentally within a factor of a few in energy of each other.

This apparent connection between the ATIC/PPB-BETS and PAMELA excesses is intriguing, but does not advance the argument that they arise from DM annihilation; it merely suggests that they arise from the *same* source, and that source produces equal numbers of e^+ and e^- . In order to distinguish DM from conventional astrophysical sources, we must look in regions where DM annihilation would produce strong signals relative to pulsars. The most obvious place for this is in the galactic center (GC) where pulsars are expected to

have a relatively uniform abundance [9, 13, 14] while the DM density is expected to rise significantly. Since the annihilation power goes as the square of the WIMP density, any production of high energy e^+e^- in the GC would likely be significantly enhanced, possibly by many orders of magnitude, for DM but not for astrophysical sources.

Remarkably, there are already indications of excess high energy electronic activity in the GC as well. Finkbeiner [15], while studying the contributions to the WMAP 1-year data, found an excess of microwave radiation termed the “WMAP Haze”. Recently, Dobler & Finkbeiner showed that the Haze persists in the WMAP 3-year data and that it is spectrally consistent with hard synchrotron emission [16]. It was first argued in [17] that this hard synchrotron radiation could possibly be produced by high energy e^+e^- products from DM annihilations. Additional studies have confirmed that the Haze *can* in fact arise from DM annihilations [18, 19], and that it would be natural for the same parameters that yield significant positron abundance in the 10-100 GeV range [19, 20].

Furthermore, previous measurements of *gamma-rays* in the GC [21] have indicated an excess above expected background levels [22] in the 10-100 GeV range. While this could arise from various sources, a very natural explanation would be from ICS of starlight photons from the same high energy e^+e^- that generate the Haze.

Building on the remarkable qualitative consistency of these data, we explore possibilities for making all of these signals from a single source of DM annihilation. The broad consistency of dark matter annihilation with all cosmic ray e^+e^- data has been studied in [23], where it was shown that the best fit points to the whole data set were in leptonic modes. Others have also noted the connections between sources of hard positrons for PAMELA [24, 25] to the higher energy signals. More recently, the connection of ATIC and decaying dark matter was studied in [26], while [27] considered the possibility of distinguishing DM and pulsar explanations with atmospheric Cherenkov telescopes. In terms of other experiments, [19] showed the consistency between positron excesses at HEAT (which is consistent with current PAMELA results) and the Haze. In this paper we argue that modes with dominant annihilation into leptons (or through a light scalar into leptons) naturally provide a good fit to *all* the data, with similar cross sections for each signal. We shall see that a robust consequence is a large signal of ICS photons towards the GC.

II. DARK MATTER AS A SOURCE OF HIGH ENERGY PARTICLES

In this section we explore the possibility that the e^+e^- , γ -ray, and microwave signals mentioned in the previous section arise from WIMP annihilation. We examine the difficulty of obtaining a high-enough cross section to leptons without violating anti-proton and π^0 γ -ray constraints, and propose a model that overcomes these difficulties.

Thermal dark matter (DM) naturally annihilates into high-energy cosmic rays, providing a source of electrons both locally and in the GC. The fact that WIMP DM naively predicts an excess of cosmic rays within a few orders of magnitudes of what is observed makes it a natural candidate for understanding the PAMELA and ATIC observations. Dark matter may annihilate through various channels, which can produce e^+e^- directly, or in decays of intermediate partners. The final particles may be detected directly by satellites or balloon experiments near Earth, or indirectly by their ICS and synchrotron signals (either locally, in the GC, in DM subhalos, or as an extragalactic background). These astrophysical signals of DM can constrain the particle mass, density, cross section, and annihilation channels.

Though this picture is appealing, attempts to explain the PAMELA excess through conventional annihilation channels (for instance to heavy flavors or gauge bosons) produce a softer positron spectrum than required [23, 28]. This problem is compounded by the absence of any anti-proton excess [29], which would have been copiously produced from these annihilation modes. At the same time, direct annihilations to leptons are a model-building challenge as Majorana fermions have helicity-suppressed annihilations to these states, forcing consideration of vector [30, 31] or Dirac [32] particles. Nonetheless, in terms of annihilations directly to standard model modes, it appears at this point that only $\chi\chi \rightarrow e^+e^-$, $\mu^+\mu^-$, $\tau^+\tau^-$ are in good agreement with the data.

An alternative mechanism was proposed by [19] as the means to produce hard leptons without anti-protons or excess π^0 's. Motivated by the requirement of a light (\lesssim GeV) boson, ϕ , in the model of [33] to explain a separate signal, they showed that annihilations $\chi\chi \rightarrow \phi\phi$, followed by $\phi \rightarrow e^+e^-$ or $\phi \rightarrow \mu^+\mu^-$ would naturally provide a hard lepton spectrum, explaining the HEAT and AMS-01 signals, and producing the Haze with similar parameters[56]. These predictions provide a good fit to the PAMELA data [25], and are a central element of a proposed unified explanation of anomalies observed by PAMELA, ATIC, INTEGRAL, and EGRET [34, 35]. Such models also naturally allow inelastic scattering,

providing a possible explanation for the DAMA annual modulation signal [36]. The light mass scale of the ϕ forbids or suppresses production of anti-protons. Furthermore, these light bosons can also help explain the amplitude of the signals by yielding the large cross section required to explain the cosmic-ray data via the Sommerfeld enhancement [34][57] or capture into bound states of “WIMPonium” [37].

In this paper, we will explore whether these annihilation channels provide a consistent picture that explains the entire set of data, including limits from the GC. We normalize our signal at the highest energies - namely ATIC and PPB-BETS - and proceed to lower energies, showing that similar parameters fit PAMELA and the Haze, while enforcing limits from EGRET. We will see that annihilations to e^+e^- , $\mu^+\mu^-$, $\phi\phi$ with $\phi \rightarrow e^+e^-$ and $\phi \rightarrow \mu^+\mu^-$ give good fits to the data. Modes with τ 's give generally too broad a peak to explain ATIC. We will also show that a natural consequence of these models is a significant ICS signal towards the GC from the scattering of starlight photons by the e^+e^- annihilation products, which may be observable by Fermi/GLAST. In the case of annihilation directly to e^+e^- , the energy cutoff of this signal should give a clear indication of the WIMP mass.

III. ANNIHILATION MODES AND THEIR COSMIC RAY SIGNALS

In this section we compute the expected cosmic-ray and photon signals for six primary annihilation modes. We consider $\chi\chi \rightarrow e^+e^-$, $\mu^+\mu^-$, and $\tau^+\tau^-$, as well as $\chi\chi \rightarrow \phi\phi$, followed by $\phi \rightarrow e^+e^-$, $\phi \rightarrow \mu^+\mu^-$, or $\phi \rightarrow \tau^+\tau^-$. For each annihilation mode, we produce a four-panel figure showing the local particle spectrum for ATIC and PAMELA, and the synchrotron and gamma-ray signals for the galactic center (Figures 3-8). We then consider the limits from diffuse gammas more generally, and estimate the astrophysical uncertainties of our predictions.

A. Analysis

Galactic cosmic ray propagation is a decades-old problem in astrophysics. Propagation parameters (diffusion and energy-loss coefficients, as well as boundary conditions) are constrained by isotope ratios of CR nuclei, measured as a function of energy. For example, the ratio of boron to carbon provides a constraint, since most carbon CRs were accelerated, but

most boron CRs were made by spallation. Likewise, ^9Be and ^{10}Be are both made by spallation, but the short half-life (1.5×10^6 yr) of ^{10}Be serves as a clock, measuring the residence time of CRs in the galaxy. Using these and other constraints, it is possible to constrain a simple cylindrical model of the Milky Way galaxy to fit existing CR data, while predicting the behavior of a new leptonic component introduced by dark matter annihilation. To do this, we use a slightly modified version of GALPROP [38] version 50.1p [58].

GALPROP computes the steady-state solution to the usual propagation equations including diffusion, re-acceleration, nuclear interactions, and energy loss to ICS, bremsstrahlung and synchrotron for electron CRs; and hadronic collisions with interstellar gas for protons and heavier nuclei. Inputs to GALPROP include 3D estimates of the starlight, far IR, and CMB energy density, gas density, magnetic field energy density, diffusion parameters, and the primary source function from “conventional” processes (e.g. SN shocks). Outputs include 3D density grids for each CR species; full-sky maps of gamma-rays due to ICS, bremsstrahlung, and π^0 gammas from ISM interactions; and a synchrotron map.

We run the code in 2D mode, solving the propagation equations on an (r, z) grid. Note that this azimuthal symmetry is imposed to obtain the steady-state CR distribution, but then skymaps are generated using the (best-guess) 3-D distributions of Galactic gas. These assumptions vastly oversimplify the Galaxy, and it is important to bear in mind that the quantitative results derived from such a model are suspect at the factor of 2 level (at least).

A recent addition to GALPROP is a feature allowing a DM profile to be specified, and the e^+e^- injected by DM annihilation to be tracked independently of other primary and secondary e^+e^- . Because the results in the inner galaxy are so important for ICS and synchrotron predictions, it is crucial to treat the central spatial bin of the GALPROP grid carefully. This pixel represents a cylinder of radius $dr = 0.1$ and height $dz = 0.05$. At a distance of 8.5 kpc, 0.1 kpc corresponds to 0.67° . Version 50.1p sub-samples each spatial bin and averages the DM density. However, the annihilation power goes as the square of the density, so it is important to compute $\langle \rho^2 \rangle$, not $\langle \rho \rangle^2$. Furthermore, the averaging code incorrectly samples the DM distribution near $r = 0$, and sometimes introduces large errors for divergent profiles.

We have fixed these problems by summing $d\Omega a^2 \rho^2 da$ over each annular (r, z) pixel, where a is the 3D radial coordinate, and $d\Omega$ is the solid angle subtended by the intersection of the pixel with a sphere of radius a . By handling this averaging carefully down to scales of

$dr/100$, we are able to obtain good convergence properties for the dr and dz given above, even for profiles as cuspy as $\rho \propto r^{-1.2}$.

In this paper, we use the Einasto profile; following Merritt et al. [39] we assume a DM halo density profile of the form

$$\rho = \rho_0 \exp \left[-\frac{2}{\alpha} \left(\frac{r^\alpha - R_\odot^\alpha}{r_{-2}^\alpha} \right) \right], \quad (1)$$

with $\rho_0 = 0.3 \text{ GeV cm}^{-3}$ as the DM density at $r = R_\odot = 8.5 \text{ kpc}$ and $r_{-2} = 25 \text{ kpc}$.

For reference, the benchmark parameters used in our runs are the following. The cylindrical diffusion zone has a radius of 16 kpc and height $\pm 4 \text{ kpc}$. The diffusion constant, $K(E) = 5.8 \times 10^{28} (E/3 \text{ GeV})^\alpha \text{ cm}^2 \text{ s}^{-1}$ where $\alpha = 0.33$ is the energy dependence expected for a turbulent magnetic field with the Kolmogorov spectrum. The rms magnetic field strength $\langle B^2 \rangle^{1/2}$, is modeled with an exponential disk,

$$\langle B^2 \rangle^{1/2} = B_0 \exp(-r/r_B - |z|/z_B) \quad (2)$$

where $r_B = 10 \text{ kpc}$ is the radial scale, $z_B = 2 \text{ kpc}$ is the vertical scale, and $B_0 = 11 \mu\text{G}$ is the value in the GC.

B. Results

The results of our analyses are presented in Figures 3-8. Qualitatively, we see that all modes considered give acceptable fits to the data. A few comments are in order, however.

The modes with annihilations directly to electrons, or ϕ -mediated electrons give the best fit to the ATIC/PPB-BETS excess. This is simply a reflection of the hardness of the injection spectra (monochromatic and flat, respectively). These modes also require the lowest boost factors. Again, this is because none of the energy is partitioned into invisible modes (as with muons or taus) or into very soft electrons and positrons (as with pions from tau decays). Direct annihilation to muons also gives an acceptable fit to the ATIC excess, while ϕ -mediated muons are slightly too soft. Annihilations to τ 's and to ϕ -mediated τ 's are significantly too soft to achieve the “peaky” nature of the excess.

A careful observer will note that there appear to be two components to the ATIC excess: a “plateau” from approximately 100-300 GeV, and a “peak” from 300-700 GeV. None of the modes we have considered independently give both of these features, but it is possible that

multiple annihilation channels could exist, for instance some linear combination of e^+e^- , $\mu^+\mu^-$ and $\tau^+\tau^-$. This could arise, for instance, if ϕ could decay into multiple states, or multiple types of ϕ particles were produced in the annihilation, as would be expected for a non-Abelian version of ϕ -mediated DM annihilation [34, 35].

All modes give a good fit for the PAMELA positron fraction. It is not unexpected, given Figure 1, that a reasonable smooth fit to ATIC also fits PAMELA. Modes with broad cutoffs (such as taus) give poor fits to ATIC, however, while modes with sharp cutoffs (electrons and ϕ -mediated electrons) give better fits, as well as smaller boost factors.

Quite remarkably, the boost factors required for the Haze are within approximately a factor of two of those needed for ATIC/PAMELA. This relationship was noted in [19], where ϕ -mediated electron and muon modes were studied as explanations for the excesses observed by previous positron cosmic ray experiments (HEAT, AMS-01). There it was found that the Haze signal naturally required a boost factor very similar to that needed for excesses that have since been seen at PAMELA.

We should note that we find larger boost factors needed for the haze than calculated in [18] (and noted in [1]). The principle reasons are the very cuspy profile used in [18], and the relatively low levels of inverse Compton scattering assumed by them.

In [18], a very cuspy profile $\rho \propto r^{-1.2}$ was used, leading to more power in the center of the galaxy, resulting in lower boost factors. In contrast, we use the Einasto profile (Eq. 1) with fits established by Merritt et al., [39]. As was shown in [19], this yields similar boost factors to an NFW profile with $\rho \propto r^{-1}$. For electrons with $E \gtrsim 5$ GeV (which, with a magnetic field of order $\sim 10\mu\text{G}$ radiate at 23 GHz), the dominant energy losses are due to ICS and synchrotron radiation. [18] considered homogeneous energy losses, and a homogeneous magnetic field of $10\mu\text{G}$. The energy loss rates used there were $5 \times 10^{-16}(E/\text{GeV})^2 \text{ GeV/s}$ and $2.5 \times 10^{-16}(E/\text{GeV})^2 \text{ GeV/s}$. As the magnetic field that we consider here has a peak value of $11\mu\text{G}$ at the center of the galaxy (corresponding to 3.0 eV cm^{-3}), our energy losses to synchrotron radiation are very similar to [18]. However, the energy losses to inverse Compton scattering increase as we get closer to the center of the galaxy, from the interstellar radiation field energy distribution, which is not expected to be homogeneous. The radiation field model used in GALPROP is large in the center, with energy densities of 18.8 eV cm^{-3} at $r = 0$ and 14.3 eV cm^{-3} at $r = 0.5 \text{ kpc}$. As a result, the larger ICS losses compete against the synchrotron losses, and less power is emitted in synchrotron radiation. This causes less

energy radiated at the 23 GHz band, resulting in higher boost factors. We note that [18] also did not include bremsstrahlung energy losses, but this has a minor effect on the overall boost.

Signals at EGRET and Fermi/GLAST

With the successful operation of Fermi/GLAST, there is naturally great interest in gamma ray signatures of dark matter models. It is especially important within the context of the present PAMELA, ATIC and PPB-BETS results, because, as we have emphasized, the galactic center may offer the ideal testing ground of the dark matter explanation of these data. It is then noteworthy that a generic prediction of scenarios involving WIMP annihilation is a significant production of ICS gamma rays in the galactic center. We believe this to be independent of the particular annihilation mode which explains ATIC and PAMELA, and only that the significant electronic production here is reflected in the galactic center.

Background cosmic rays in the galactic center are expected to come from a variety of sources. Specifically, π^0 's from protons interacting with the ISM, inverse Compton scattering (ICS) from cosmic ray electrons, as well as a small component of bremsstrahlung. (See Figure 2.) Note that the conventional sources are expected to fall dramatically as one moves to higher energies.

In context of our present discussion, this should be dramatically changed. If dark matter is responsible for an $O(1)$ correction to cosmic ray electrons locally in the 400-800 GeV range, then it would be expected to dominate this energy range in the galactic center. Such electrons are responsible for upscattering photons to energies $E_{upscatter} = 2E_{initial}\gamma^2$. For (initially) optical photons, this will result in a major contribution to photons in the 10 - 1000 GeV range. Note that these photons are independent of other sources, such as the final-state radiation (FSR) gammas from charged particle production or π^0 's produced in e.g., τ decay. Rather, these photons are intimately linked to the production of high-energy electrons and positrons. The same population of particles which we believe should be yielding the haze.

Indeed, this basic intuition is borne out in Figures 3-8. One sees very significant gamma ray signatures at high energies in all channels. One should not read too much into the fact that many modes seem to exceed the EGRET values - as we shall discuss shortly, there is a factor of a few uncertainty in this arising from astrophysics. While modes with τ 's can have this be dominated by π^0 production (often exceeding present EGRET limits quite signifi-

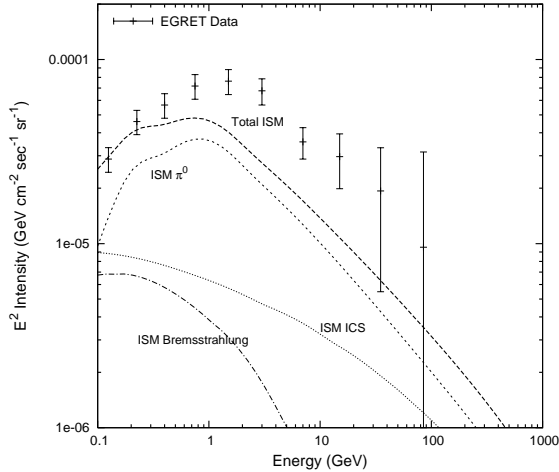


FIG. 2: The dominant contributions to gamma rays in the galactic center (inner 5°) from conventional astrophysical CR interactions. Shown are the photons from π^0 's, electron ICS signals and bremsstrahlung. In this and following figures, “ISM” denotes gammas produced by CR interactions with the interstellar radiation field, as well as the interstellar medium (gas and dust). The π^0 line refers to π^0 γ -rays produced by the hadronic CRs interacting with the interstellar medium. The slope of the π^0 curve at high energies is tied to the primary p CR spectrum, and is better constrained than the amplitude.

cantly), the contributions from electron and muon modes is dominated by ICS. FSR signals only tend to be significant at the highest energies (out of the range of Fermi/GLAST), and do depend on the parameters involved (notably the ϕ mass in the ϕ -mediated modes). Furthermore, the collinear approximation we have used for the FSR gammas is not appropriate at the highest energies, where FSR becomes important, and should probably be taken as an upper bound on the FSR signal in that energy range. That said, it is possible that a lower value for the ISRF energy density could lead to a lower ICS signal as we shall discuss shortly, in which case FSR signals could be quite relevant in the Fermi range. The size and shape of the FSR signal will also be model dependent. In contrast, the ICS signal should be present for any population of electrons with the same spectrum which explains ATIC and PAMELA, and, more to the point, almost any population of DM produced electrons which explains the Haze. This strong signal should be observed by Fermi/GLAST and would be a smoking gun of this massive high energy electronic production in the galactic center.

We note that none of our current models seem to give a good fit to the EGRET data

points in the 2 – 5 GeV range. This difficulty these observations with standard mechanisms was pointed out previously by [22], who proposed an “optimized” model, with a modified electron and proton CR spectrum. Because this excess appears everywhere on the sky, not just the galactic center, it is unlikely to be related to ICS from dark matter. A modified proton spectrum is also not likely in our model, given that no significant anti-proton excess has been observed. However, the potential for DM annihilation to affect the average electron spectrum is obvious.

C. Limits from diffuse gamma rays

One of the most important consequences of this scenario is the presence of significant ICS gamma ray production in the inner few degrees of the galaxy. This is a natural byproduct of these new sources of e^+e^- , these signals are naturally dependent on the positrons and electrons produced, and hence on the cosmic ray propagation models. In contrast, predictions of photons from π^0 's or final state radiation [43, 44] are much more robust, because they depend only on the DM halo profile and annihilation modes. It is worth considering the constraints these prompt photons place on DM annihilation, using both galactic center and diffuse extra-galactic limits.

We show in Figure 10 the limits on boost factors (BF) for different γ production modes, both for NFW and Einasto profiles. To generate these plots, we calculate the total flux of prompt photons, either from FSR or π^0 decays from the different sky regions given by [41]. We consider annihilations to $\tau\tau$, $\pi^0\pi^0$, as well as the FSR signals associated with e^+e^- , as well as the mediator decay modes $\chi\chi \rightarrow \phi\phi$, with $\phi \rightarrow \tau^+\tau^-$, $\phi \rightarrow \pi^0\pi^0$ and $\phi \rightarrow e^+e^-$. To generate these limits, we use the EGRET bounds from [41], and take the 2-sigma upper bounds to be conservative (no background subtraction is included). We show limits for both NFW (dashed) and Einasto (solid) profiles. Since NFW limits typically come from interior regions while Einasto limits typically come from extra-galactic data, alternative profiles may yield yet weaker limits.

Other limits can be found from HESS data [43] or from the inner 1° of the Milky Way. These limits are highly dependent on the details of the profile, and we limit ourselves to the more conservative ones from the EGRET data.

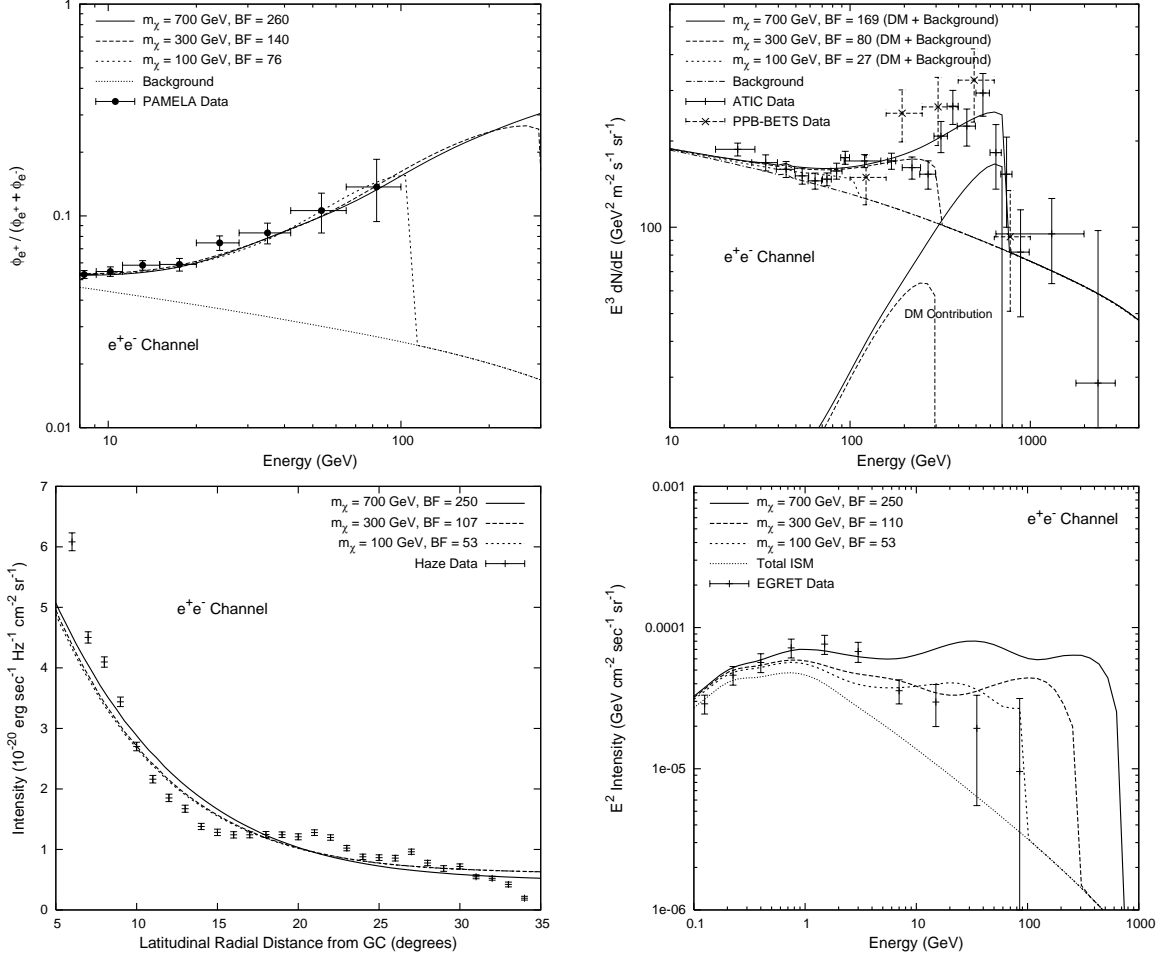


FIG. 3: The cosmic ray signals from dark matter annihilations $\chi\chi \rightarrow e^+e^-$. *Upper left:* predicted positron fraction vs. energy (*solid line*), expected secondary spectrum (*dashed*) and PAMELA [5] data points. BF is the boost factor required relative to $\langle\sigma_A v\rangle = 3 \times 10^{-26}$ cm³/s and the reference local DM density of $\rho_0 = 0.3$ GeV cm⁻³. *Upper right:* spectrum of DM (e^+e^-) (*dotted*), background signal (*dashed*), and total (*solid*) with data from ATIC [1] and PPB-BETS [3]. *Lower left:* Predicted WMAP haze signal vs. galactic latitude at 23 GHz (*solid*) and data points from WMAP [16]. Error bars are statistical only. *Lower right:* Diffuse gamma ray spectrum in the inner 5° of the Milky Way, computed with GALPROP [40]. FSR = Final State Radiation. Data points are from the Strong et al. re-analysis of the EGRET data [41], which found a harder spectrum at 10 – 100 GeV within a few degrees of the GC, using improved sensitivity estimates from [42].

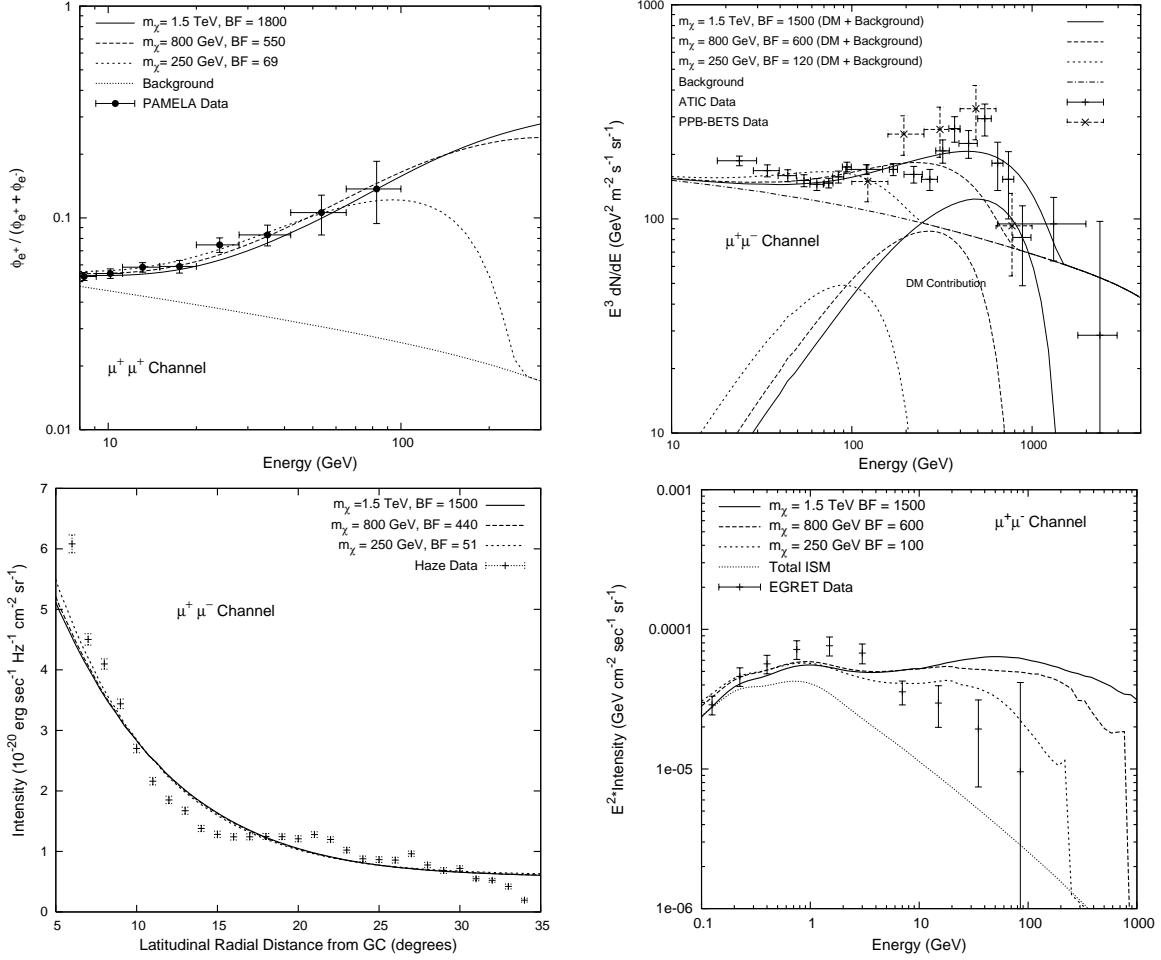


FIG. 4: The cosmic ray signals of dark matter annihilations as in Fig. 3, but with $\chi\chi \rightarrow \mu^+\mu^-$.

D. Other modes

While we have focused on the six simple modes, there are many alternatives. In particular, if ϕ is a vector, it can go to combinations of various modes [25, 34]. These tend to have little effect on PAMELA and ATIC [25], which are dominated by the hardest significant mode. Similarly, the Haze, which is dictated by the same energy ranges as PAMELA, is not extremely sensitive.

However, the presence of additional soft electrons and positrons can change the spectrum of ICS photons. As an example we show in Figure 11 the case of annihilations $\chi\chi \rightarrow \phi\phi$ where ϕ decays to e^+e^- , $\mu^+\mu^-$ and $\pi^+\pi^-$ in a 4:4:1 ratio. We see that some improvement can be had at lower ($\sim 1 - 10$ GeV) photon energies.

Similarly, we can consider how well an annihilation mode with hadronic elements can

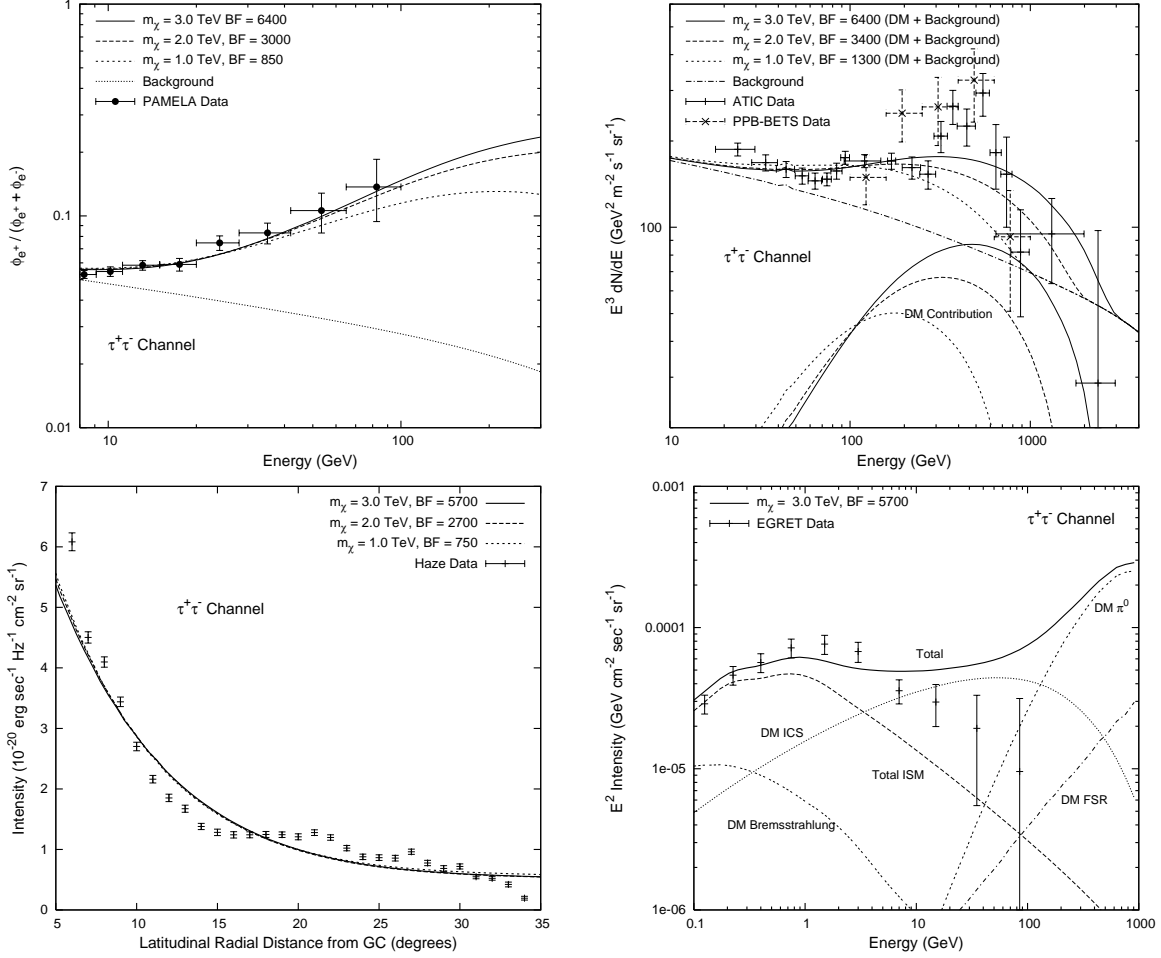


FIG. 5: The cosmic ray signals of dark matter annihilations $\chi\chi \rightarrow \tau^+\tau^-$.

fit the data. We show in Figure 12 the signal of $\chi\chi \rightarrow WW$. Such a mode is strongly excluded by anti-protons [45, 46], but is still instructive to see how modes with significant soft components fit the data. An approximately 1 TeV WIMP gives the best fit to the ATIC data (dominantly through its hard leptonic decays), but even this does a poor job of reproducing the spectrum. Going to higher masses does not help. At lower energies the positrons would significantly overproduce the PAMELA data, and provide a poor fit even with smaller boost factors (note that the approximate fits to the PAMELA data have boosts only half as large as those at ATIC). Extragalactic limits on diffuse gammas are stronger than this, as discussed by [47], where boosts of ~ 100 were found to be borderline with EGRET within the context of an NFW profile. Together with the strong \bar{p} limits, any explanation with W bosons would be expected to be due to a significant local production.

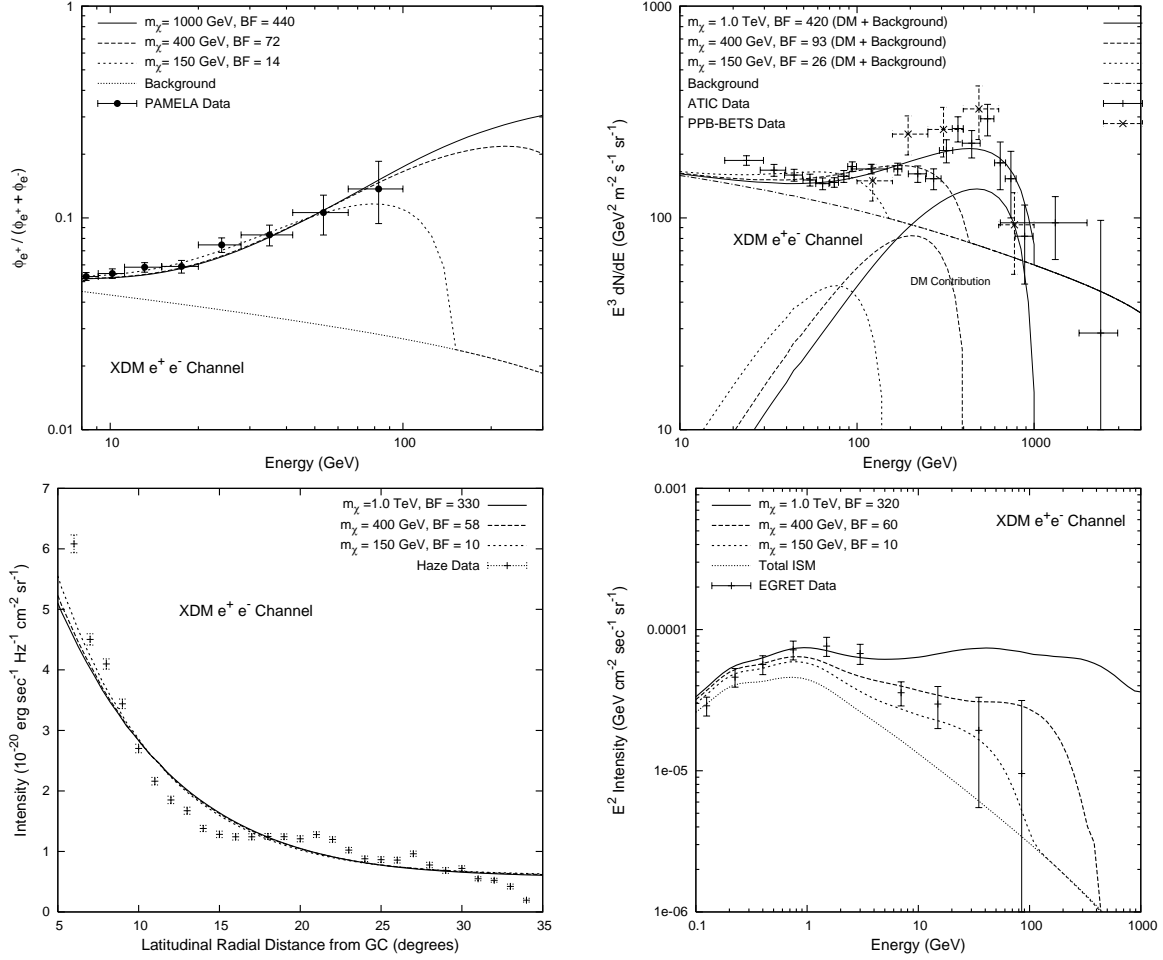


FIG. 6: The cosmic ray signals of dark matter annihilations $\chi\chi \rightarrow \phi\phi$, followed by $\phi \rightarrow e^+e^-$.

Consequently, neither a haze nor an ICS signal would be expected (as the similar boost would not be expected in the center of the galaxy).

Finally, if the ϕ is a scalar, then one can expect a branching ratio to $\gamma\gamma$ up to $\sim 10\%$ [19]. We show how such a contribution to the Fermi/GLAST signal would appear in Figure 13. One can see that in their Fermi range, the γ 's are swamped by ICS and FSR contributions. Only at the highest energies is this visible. Should ATIC not arise from dark matter, and if the ϕ is sufficiently light ($\lesssim 300$ GeV) it may appear as a small peak at the end of the E^2 gamma distribution (as the spectrum of these photons is flat in energy). However, even there, it will be difficult to extract from FSR.

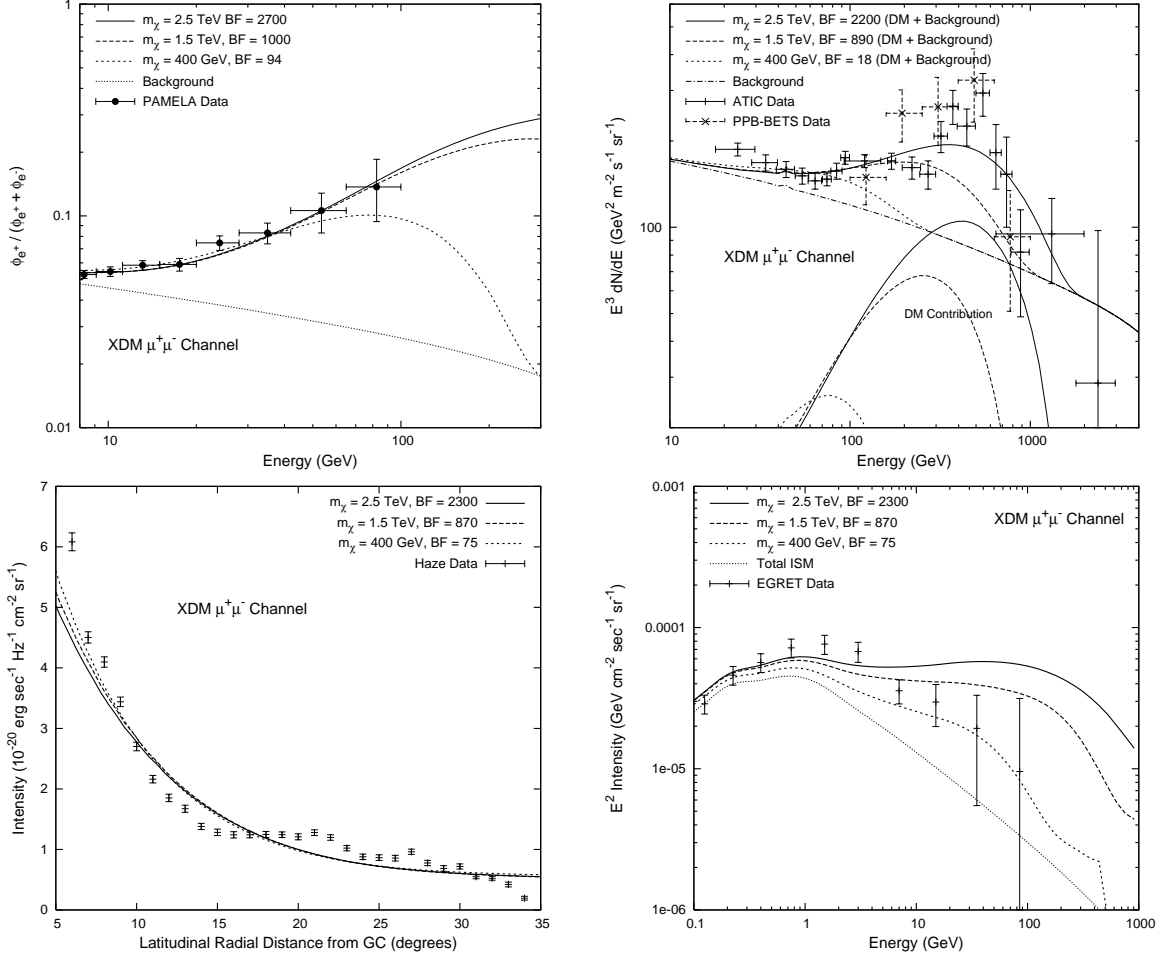


FIG. 7: The cosmic ray signals of dark matter annihilations $\chi\chi \rightarrow \phi\phi$, followed by $\phi \rightarrow \mu^+\mu^-$.

E. Astrophysical Uncertainties

One of the most robust predictions of the dark matter scenarios considered above is the ICS signal in the center of the galaxy. One might naturally wonder how robust this is.

The greatest source of uncertainty is the extrapolation of the local annihilation signal, as observed by PAMELA and ATIC, to the galactic center. This extrapolation is uncertain for many reasons, not least because of the assumption of a smooth dark matter distribution in the galactic halo, in spite of the fact that simulations show clumpy substructure. Dark matter in subhalos, which might ordinarily be comparable to the annihilation power from the smooth halo even in conventional models, can dominate by a large factor in the case of Sommerfeld enhanced annihilation [34], because the velocity dispersion of subhalos is small. In this case the annihilation power in the galactic center has more to do with the mass

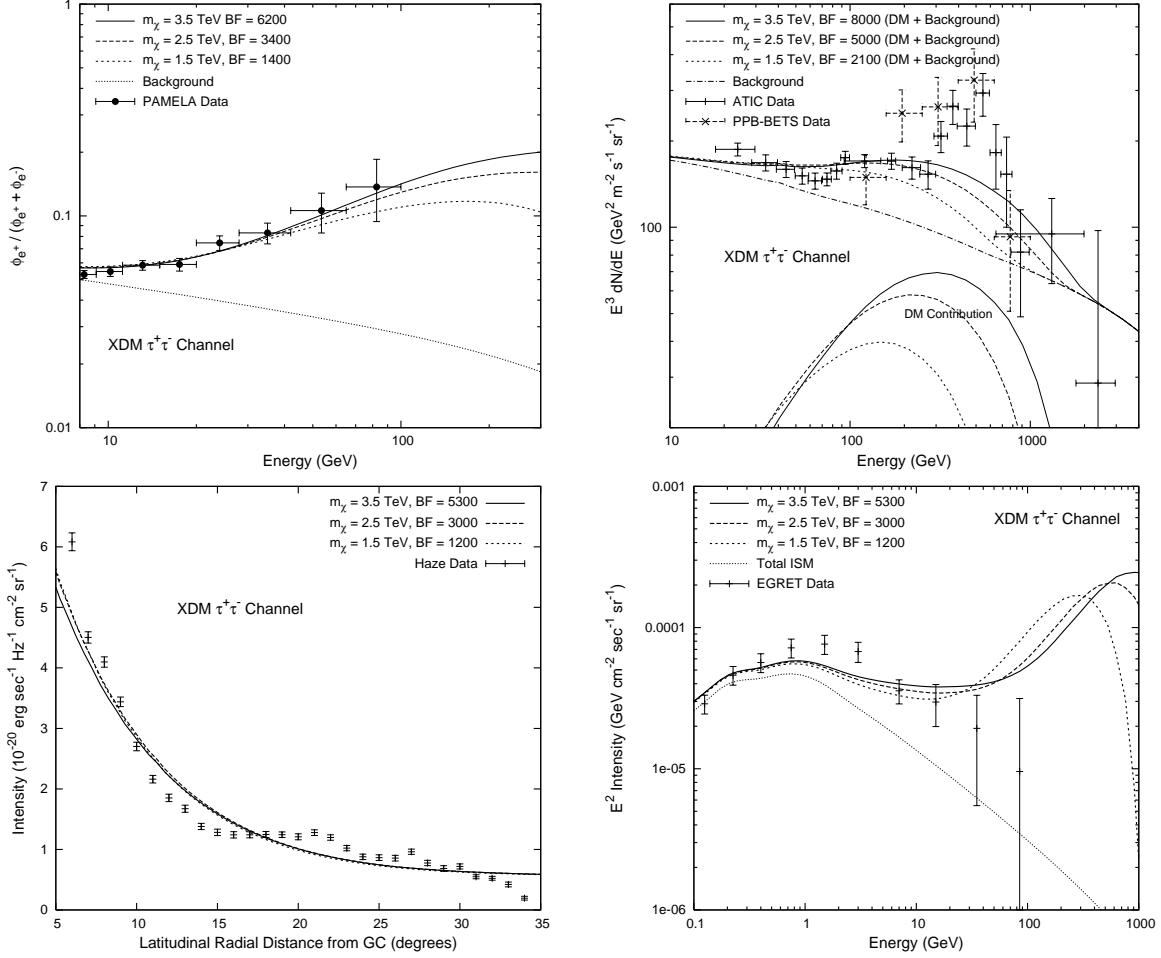


FIG. 8: The cosmic ray signals of dark matter annihilations $\chi\chi \rightarrow \phi\phi$, followed by $\phi \rightarrow \tau^+\tau^-$.

distribution and survival rate of clumps in the center than the properties of the smooth halo. In other cases, the dark matter can form a dark disk, leading to high annihilation rates [48]. On the other hand, the halo could be less cuspy than we've assumed here, and substructure could be destroyed in the center, lowering the annihilation signal relative to our expectations. Taking into account the uncertainties in both the dark matter distribution and the particle physics, our simple extrapolation from local annihilation rate to the galactic center is probably uncertain by one or two orders of magnitude.

However, if the central density is too low, we would be unable to explain the Haze with annihilations, or the 511 keV signal from INTEGRAL through the exciting dark matter mechanism. But it happens that the boosts needed to explain the Haze are very similar to those needed for ATIC and PAMELA, and so we constrain most of these uncertainties

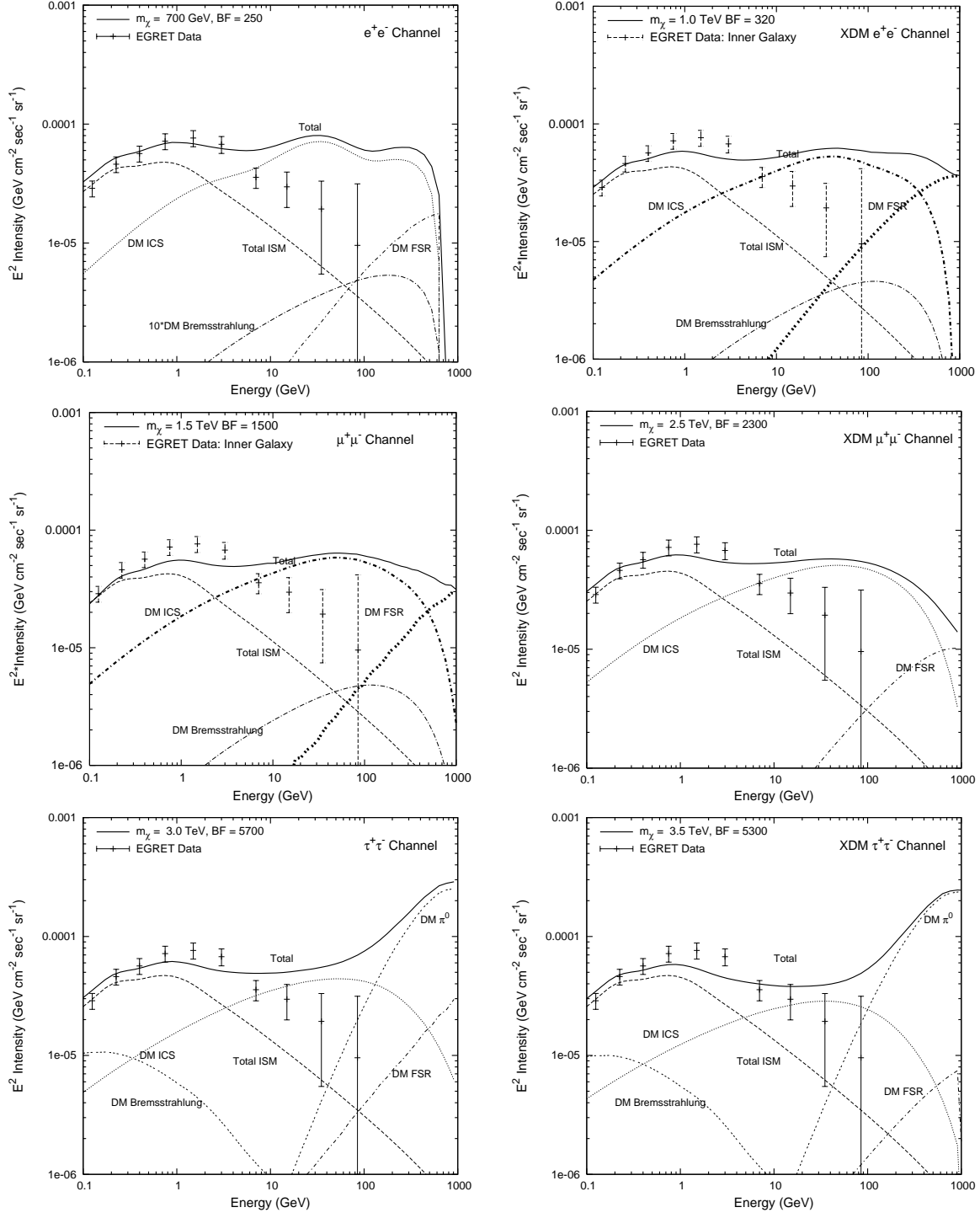


FIG. 9: Different contributions to gamma rays in the galactic center for different dark matter annihilation modes.

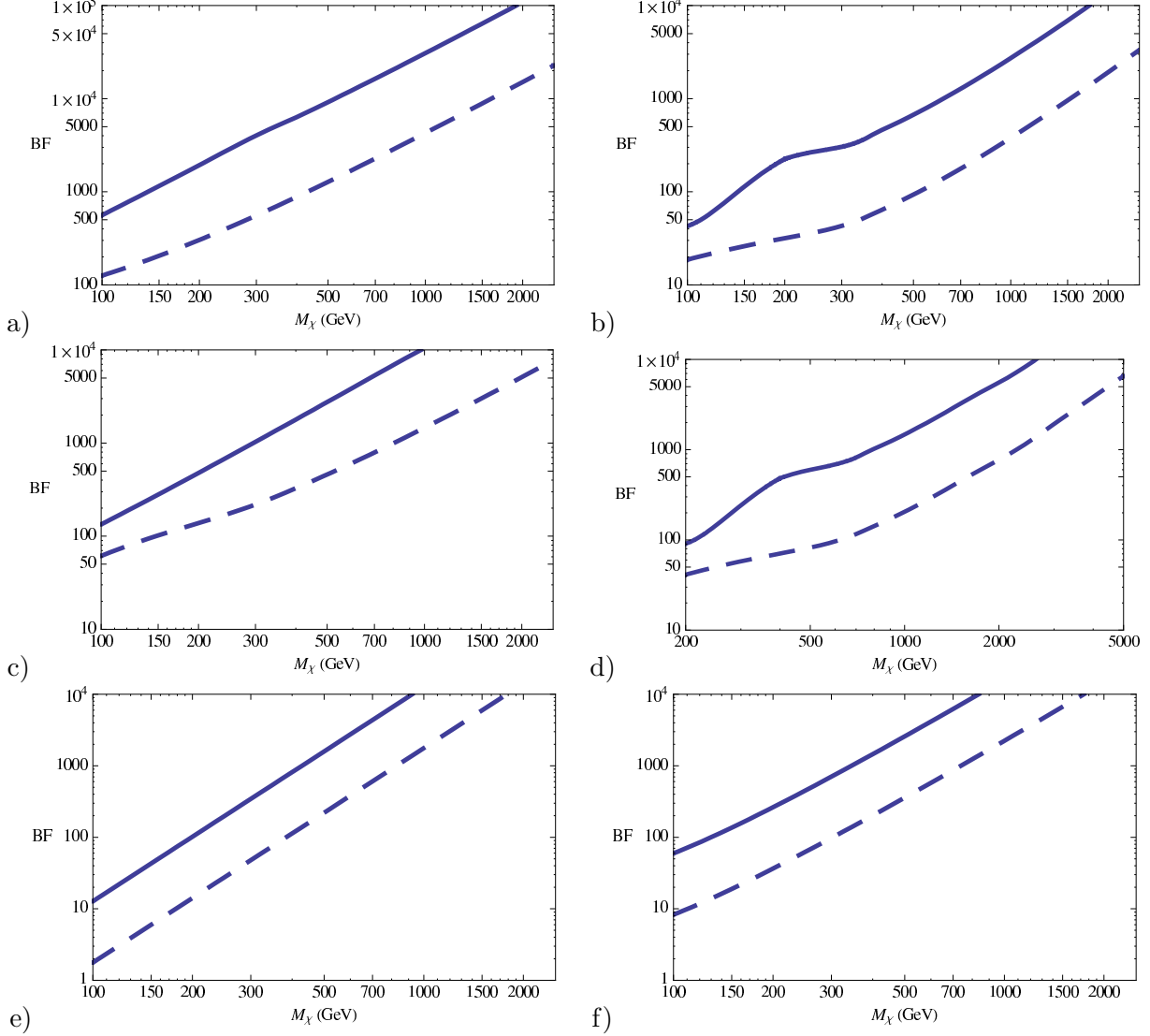


FIG. 10: Boost factor limits (compared to $\sigma v = 3 \times 10^{-26} \text{ cm}^3 \text{ s}^{-1}$ and $\rho_0 = 0.3 \text{ GeV cm}^{-3}$ for a) $\chi\chi \rightarrow e^+e^-$, b) $\chi\chi \rightarrow \tau^+\tau^-$, c) $\chi\chi \rightarrow \phi\phi$, $\phi \rightarrow e^+e^-$, d) $\chi\chi \rightarrow \phi\phi$, $\phi \rightarrow \tau^+\tau^-$, e) $\chi\chi \rightarrow \pi^0\pi^0$, f) $\chi\chi \rightarrow \phi\phi$, $\phi \rightarrow \pi^0\pi^0$. Dashed lines correspond to limits from an NFW profile, while solid lines correspond to limits from an Einasto profile. The limits come from prompt FSR and π^0 gammas only. Limits are determined by requiring that no EGRET data point is exceeded by more than 2σ .

using the normalization of the Haze. This still is not perfect; there is always a factor of ~ 2 uncertainty in the boosts associated with the Haze, simply arising from uncertainties in the strength of the magnetic field in the galactic center.

Putting aside this uncertainty, we can examine the range of signals possible for Fermi/GLAST. To do this, it is important to distinguish the different components con-

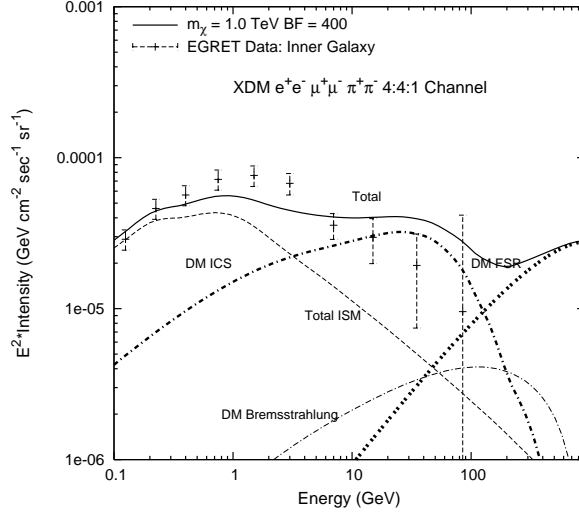


FIG. 11: The gamma ray signals from a model that annihilates into electrons, muons, and pions in a 4:4:1 ratio. The gamma ray spectrum is noticeably softer than that for annihilations into just electrons with the same mass.

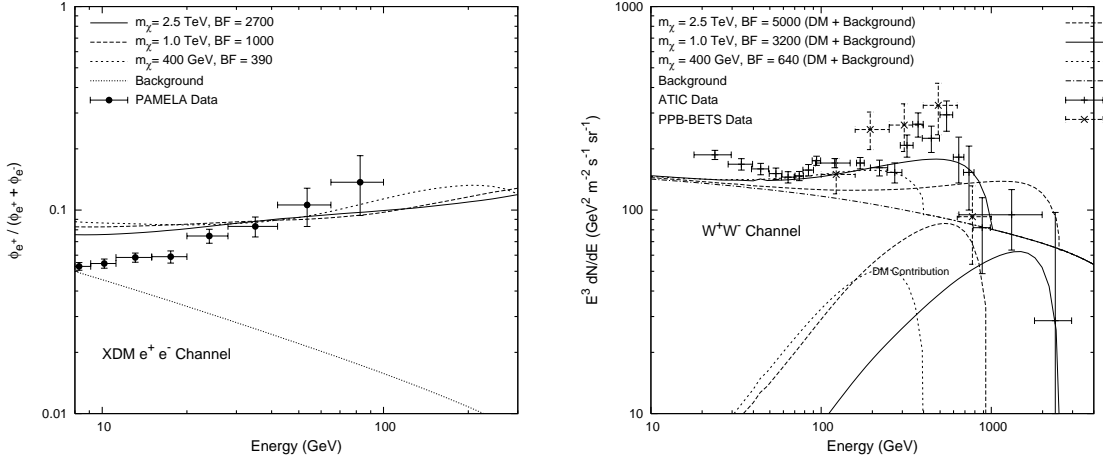


FIG. 12: PAMELA and ATIC signals of dark matter annihilations $\chi\chi \rightarrow W^+W^-$.

tributing to the Fermi DM signal, namely, ICS, FSR and π^0 gammas. The π^0 gammas arise only from the modes with τ 's, but all the modes we consider have an FSR signal, whether the annihilation goes directly into charged particles or via intermediate ϕ states (see appendix). Given a WIMP model, these photons (FSR and π^0) are uncertain only at the level of the overall dark matter annihilation in the galactic center, which is naturally the appropriate size to produce the Haze.

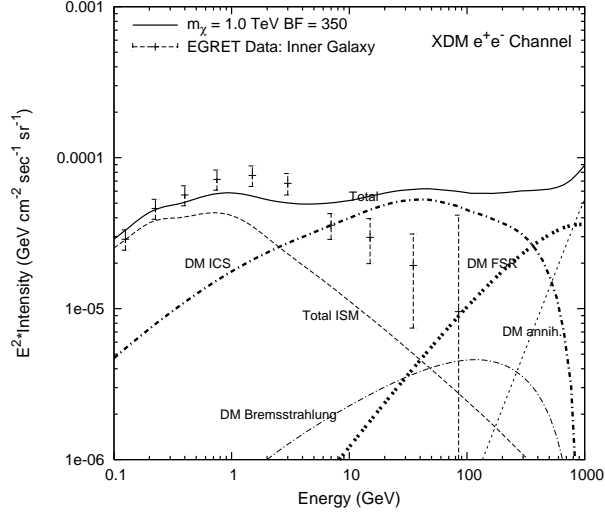


FIG. 13: Gamma ray signals including a 10% BR of $\phi \rightarrow \gamma\gamma$.

The ICS photons are also produced by all the modes under consideration, and are, in general, the most model-independent prediction of these scenarios, arising directly from the interactions of electrons and positrons with starlight. This, however, can vary significantly, because the electrons share their energy between ICS and synchrotron, depending on the relative energy density of starlight vs. the magnetic field. If the magnetic field in the galactic center is larger than the $11\mu\text{G}$ we assume ($= 3 \text{ eV cm}^{-3}$), then this increases the signal in WMAP, at the expense of the ICS signal, assuming constant power. If the annihilation power is normalized to the Haze, then the inferred ICS power drops further. Additionally, by changing the diffusion constant, we can trap more or fewer of the electrons in the galactic center region for different periods, allowing more signal to propagate away from the inner 5° . Finally, if the energy density of starlight is lower than used in the ISRF maps employed in GALPROP, this can also decrease the signal by a corresponding factor of up to roughly two at higher energies. We attempt to quantify these uncertainties in the Figure 14 for the ICS signal from $\chi\chi \rightarrow \phi\phi$, with $\phi \rightarrow e^+e^-$. We see that the signal can be suppressed by a factor of 3-6, depending on energy.

The dominant gamma ray contribution for most modes is from ICS, as we show in Figure 9. Aside from this contribution and its uncertainty, we see, for the tau modes, there is significant production of gamma ray radiation from π^0 gammas. Normalizing to the haze, we expect a possibility of variation in this contribution at roughly a level of a factor of 2,

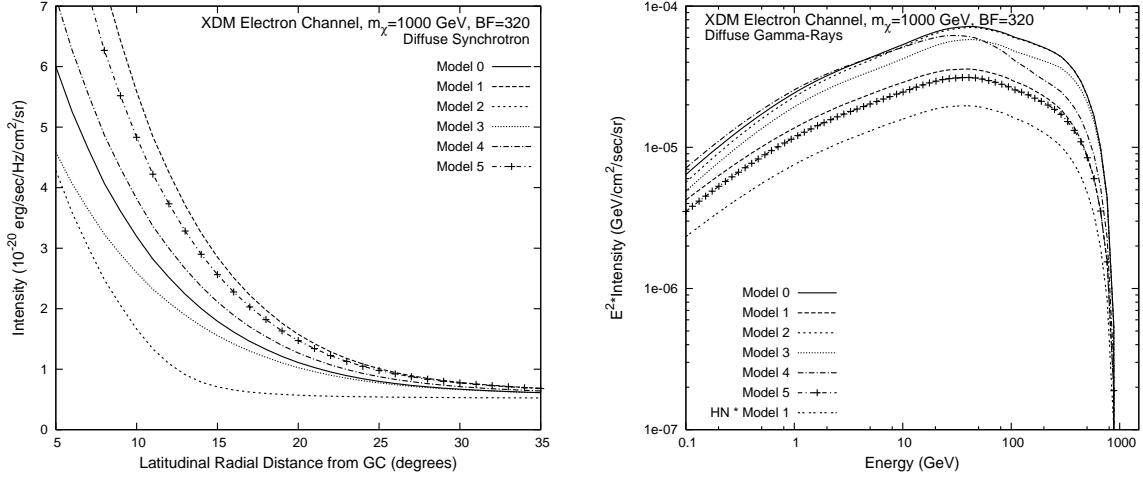


FIG. 14: Synchrotron (as a function of radial distance from the GC, *left*) and ICS (*right*) towards the GC for five different diffusion models. Model 0: the “benchmark” model given in §III A. Model 1: B_0 doubled leading to more energy losses from synchrotron compared to ICS. Model 2: Diffusion zone scale height decreased from 4 kpc to 2 kpc. Model 3: Diffusion index, α , changed from 0.33 (Kolmogorov spectrum) to 0.5. Model 4: Optical intensity in the interstellar radiation field reduced by half leading to less ICS of optical photons (decreased ICS at energies above 10 GeV) and increased synchrotron. Model 5: B_0 doubled *and* α increased from 0.33 to 0.5. Since Model 1 yields the largest synchrotron output, if we normalize the boost factor to fit the haze data with this model, the implied ICS (“HN * Model 1”) emission is roughly a factor of 3-4 below the “benchmark” Model 0.

that is, just in proportion to the overall changes in DM annihilation needed for the haze. A similar level of uncertainty can be made for the FSR gammas, although they are less important. Thus, explaining the existing data (Haze+ATIC+PAMELA) with dominant tau modes seems in significant tension with existing EGRET data. This should be easily clarified by Fermi/GLAST, however.

IV. CONCLUSIONS

The excesses of electronic production at $\sim 400 - 800$ GeV observed by earlier experiments of ATIC and PPB-BETS have now been confirmed by the recent run of ATIC. This gives a new piece of evidence of a new primary source of electronic production in the halo. Recent

results by the PAMELA experiment point in a similar direction. Simple extrapolations of PAMELA seem to connect the two experiments, calling out for consideration of a unified explanation.

In this paper, we have studied the possibility that dark matter annihilations could explain simultaneously the excesses seen by ATIC/PPB-BETS, PAMELA and WMAP. We find remarkable agreement, with very similar boost factors to explain each one of them. The presence of the Haze in the center of the galaxy, gives some weight to the dark matter interpretation of the signal, as astrophysical sources would not be expected to give significant positron fluxes in the galactic center, much less at latitudes of 5° to 10° (700pc to 1400 pc) off the galactic disk. The Fermi/GLAST observations of ICS and other photons in the galactic center should give clear evidence for this scenario. Should these gamma rays extend to the reach of the Fermi/LAT experiment, the ubiquity and scale of excess electronic production would make dark matter the definitive explanation.

Acknowledgements

We would like to acknowledge helpful discussions with Tracy Slatyer. DPF and GD are partially supported by NASA LTSA grant NAG5-12972. This work was partially supported by the Director, Office of Science, of the U.S. Department of Energy under Contract No. DE-AC02-05CH11231. NW is supported by NSF CAREER grant PHY-0449818. LG, IC and NW are supported by DOE OJI grant #DE-FG02-06E R41417. NW acknowledges the hospitality and support of the Kavli Institute for Theoretical Physics China, CAS, Beijing 100190, China, where some of this work was undertaken.

APPENDIX A: FINAL STATE RADIATION

Final state radiation is very important for annihilations into charged states [43, 44, 49, 50]. An exhaustive study of FSR is well beyond our purposes here, but we include it in the spectra presented. The FSR for the dark matter direct annihilation to fermions is [44]

$$\frac{d\sigma(\chi\chi \rightarrow f\bar{f}\gamma\gamma)}{dx} \approx \frac{\alpha Q_f^2}{\pi} \mathcal{F}(x) \log\left(\frac{s(1-x)}{m_f^2}\right) \sigma(\chi\chi \rightarrow f\bar{f}) \quad (\text{A1})$$

where $s = 4m_\chi^2$, $x = 2E\gamma/\sqrt{s}$, and $\mathcal{F}(x) = ((1-x)^2 + 1)/x$.

For the decays of $\phi \rightarrow f\bar{f}$, we need a slightly different formula.

Working from eq. A1, we can instead consider the case of ϕ decay, which has the same essential formula, but with $s = m_\phi^2$. If ϕ is boosted by an amount $\gamma = m_\chi/m_\phi$. If we assume the γ is emitted at angle θ relative to the boost, we have the relationship

$$y = \frac{E_\gamma}{m_\chi} = \frac{x}{2}(1 + \cos \theta) \quad (\text{A2})$$

Then we have a distribution of γ 's for every ϕ

$$\frac{dN}{dy} = \frac{1}{2} \int_{\cos \theta_{min}}^1 d \cos \theta \frac{dN}{dx} \frac{dx}{dy} \quad (\text{A3})$$

where $\cos \theta_{min} = 2y - 1$. This gives

$$\frac{dN}{dy} = \frac{\alpha Q_f^2}{2\pi} \int_{\cos \theta_{min}}^1 \frac{1}{y} (1 + (1 - x)^2) (\log(m_\phi^2/m_f^2) + \log(1 - x)) \quad (\text{A4})$$

The first term, proportional to $\log(m_\phi^2/m_f^2)$, is dominant at small x , and is easily evaluated, while the second is somewhat more complicated. We write this as

$$\frac{dN}{dy} = \frac{\alpha Q_f^2}{y\pi} (\log(m_\phi^2/m_f^2) P_1 + P_2), \quad (\text{A5})$$

where

$$P_1 = 2 - y + 2y \log y - y^2 \quad (\text{A6})$$

and

$$\begin{aligned} P_2 = & -\log(1 - y)y^2 + y^2 + \log^2(2y)y + \frac{1}{2} \log(16) \log\left(1 - \frac{1}{y}\right) y \\ & - \log(2 - 2y)y - 2 \log(2) \log(1 - y)y - 2 \log\left(\frac{1}{y}\right) y \\ & - 2 \log\left(-\frac{1}{y}\right) \log(2y)y + 2 \log\left(\frac{1}{y}\right) \log(2y)y + 2 \text{Li}_2\left(\frac{1}{y}\right) y \\ & + \frac{1}{2} \log(4)y - \log^2(2)y - \frac{\pi^2 y}{3} - y + \log(2 - 2y) \\ & + \log(1 - y) + 2 \log\left(\frac{1}{y}\right) + 2 \log(2y) - \frac{\log(64)}{6} - 2 \log(2) \\ & - \frac{\log\left(\frac{1}{y}\right)}{2y} - \frac{\log(2y)}{2y} + \frac{\log(2)}{2y} \end{aligned} \quad (\text{A7})$$

A few points to consider: one must of course recall that this is the γ distribution per ϕ , and thus that are two ϕ 's per annihilation. Also, we have used the approximate formula A1,

which is only valid in the collinear limit. The hardest part of the spectrum we show would then be expected to be somewhat softer than what we have displayed. A complete analysis is warranted.

-
- [1] J. Chang et al., *Nature* **456**, 362 (2008).
 - [2] J. Chang et al. (ATIC) (2005), prepared for 29th International Cosmic Ray Conferences (ICRC 2005), Pune, India, 31 Aug 03 - 10 2005.
 - [3] S. Torii et al. (2008), 0809.0760.
 - [4] P. Picozza et al., *Astropart. Phys.* **27**, 296 (2007), astro-ph/0608697.
 - [5] O. Adriani et al. (2008), 0810.4995.
 - [6] S. W. Barwick et al. (HEAT), *Astrophys. J.* **482**, L191 (1997), astro-ph/9703192.
 - [7] M. Aguilar et al. (AMS-01), *Phys. Lett. B* **646**, 145 (2007), astro-ph/0703154.
 - [8] F. A. Aharonian, A. M. Atoyan, and H. J. Volk, *Astron. Astrophys.* **294**, L41 (1995).
 - [9] L. Zhang and K. S. Cheng, *Astron. Astrophys.* **368**, 1063 (2001).
 - [10] L. Zhang and K. S. Cheng, *Astron. Astrophys.* **368**, 1063 (2001).
 - [11] D. Hooper, P. Blasi, and P. D. Serpico (2008), 0810.1527.
 - [12] H. Yuksel, M. D. Kistler, and T. Stanev (2008), 0810.2784.
 - [13] B. Paczynski, *Astrophys. J.* **348**, 485 (1990).
 - [14] S. J. Sturmer and C. D. Dermer, *Astrophys. J.* **461**, 872 (1996).
 - [15] D. P. Finkbeiner, *Astrophys. J.* **614**, 186 (2004), astro-ph/0311547.
 - [16] G. Dobler and D. P. Finkbeiner (2007), arXiv:0712.1038 [astro-ph].
 - [17] D. P. Finkbeiner (2004), astro-ph/0409027.
 - [18] D. Hooper, D. P. Finkbeiner, and G. Dobler, *Phys. Rev. D* **76**, 083012 (2007), arXiv:0705.3655 [astro-ph].
 - [19] I. Cholis, L. Goodenough, and N. Weiner (2008), 0802.2922.
 - [20] P. Grajek, G. Kane, D. J. Phalen, A. Pierce, and S. Watson (2008), arXiv:0807.1508 [hep-ph].
 - [21] D. Hooper and B. L. Dingus, *Phys. Rev. D* **70**, 113007 (2004), astro-ph/0210617.
 - [22] A. W. Strong, I. V. Moskalenko, and O. Reimer, *Astrophys. J.* **613**, 962 (2004), astro-ph/0406254.
 - [23] M. Cirelli, M. Kadastik, M. Raidal, and A. Strumia (2008), 0809.2409.

- [24] A. E. Nelson and C. Spitzer (2008), 0810.5167.
- [25] I. Cholis, D. P. Finkbeiner, L. Goodenough, and N. Weiner (2008), 0810.5344.
- [26] C.-R. Chen, F. Takahashi, and T. T. Yanagida (2008), 0811.3357.
- [27] J. Hall and D. Hooper (2008), 0811.3362.
- [28] I. Cholis, L. Goodenough, D. Hooper, M. Simet, and N. Weiner (2008), 0809.1683.
- [29] O. Adriani et al. (2008), 0810.4994.
- [30] H.-C. Cheng, J. L. Feng, and K. T. Matchev, Phys. Rev. Lett. **89**, 211301 (2002), hep-ph/0207125.
- [31] D. Hooper and G. D. Kribs, Phys. Rev. **D70**, 115004 (2004), hep-ph/0406026.
- [32] R. Harnik and G. D. Kribs (2008), 0810.5557.
- [33] D. P. Finkbeiner and N. Weiner, Phys. Rev. **D76**, 083519 (2007), astro-ph/0702587.
- [34] N. Arkani-Hamed, D. P. Finkbeiner, T. Slatyer, and N. Weiner (2008), 0810.0713.
- [35] N. Arkani-Hamed and N. Weiner (2008), 0810.0714.
- [36] S. Chang, G. D. Kribs, D. Tucker-Smith, and N. Weiner (2008), 0807.2250.
- [37] M. Pospelov and A. Ritz (2008), 0810.1502.
- [38] I. V. Moskalenko and A. W. Strong, Phys. Rev. **D60**, 063003 (1999), astro-ph/9905283.
- [39] D. Merritt, J. F. Navarro, A. Ludlow, and A. Jenkins, Astrophys. J. Lett. **624**, L85 (2005), astro-ph/0502515.
- [40] A. W. Strong and I. V. Moskalenko (1999), astro-ph/9906228.
- [41] A. W. Strong et al., Astron. Astrophys. **444**, 495 (2005), astro-ph/0509290.
- [42] D. J. Thompson, D. L. Bertsch, and R. H. O’Neal, Jr., Astrophys. J. Supp. **157**, 324 (2005), arXiv:astro-ph/0412376.
- [43] N. F. Bell and T. D. Jacques (2008), 0811.0821.
- [44] A. Birkedal, K. T. Matchev, M. Perelstein, and A. Spray (2005), hep-ph/0507194.
- [45] M. Cirelli, R. Franceschini, and A. Strumia, Nucl. Phys. **B800**, 204 (2008), 0802.3378.
- [46] F. Donato, D. Maurin, P. Brun, T. Delahaye, and P. Salati (2008), 0810.5292.
- [47] E. A. Baltz et al., JCAP **0807**, 013 (2008), arXiv:0806.2911 [astro-ph].
- [48] J. I. Read, G. Lake, O. Agertz, and V. P. Debattista (2008), 0803.2714.
- [49] J. F. Beacom, N. F. Bell, and G. Bertone, Phys. Rev. Lett. **94**, 171301 (2005), astro-ph/0409403.
- [50] G. D. Mack, T. D. Jacques, J. F. Beacom, N. F. Bell, and H. Yuksel, Phys. Rev. **D78**, 063542

- (2008), 0803.0157.
- [51] M. Pospelov, A. Ritz, and M. B. Voloshin (2007), arXiv:0711.4866 [hep-ph].
 - [52] J. Hisano, S. Matsumoto, and M. M. Nojiri, Phys. Rev. Lett. **92**, 031303 (2004), hep-ph/0307216.
 - [53] J. Hisano, S. Matsumoto, M. M. Nojiri, and O. Saito, Phys. Rev. **D71**, 063528 (2005), hep-ph/0412403.
 - [54] M. Cirelli and A. Strumia (2008), arXiv:0808.3867 [astro-ph].
 - [55] see Fig. s8 in the Supplement to [1]
 - [56] See [51] for a discussion of the general class of “secluded” WIMP models which includes this as a subset.
 - [57] The importance of this effect in the context of multi-TeV scale dark matter interacting via W and Z bosons was first discussed by [52, 53], and more recently emphasized with regards to PAMELA in the context of “minimal dark matter,” with similar masses by [45, 54].
 - [58] GALPROP and the resource files we employed are available at <http://galprop.stanford.edu>; our modifications are available upon request.